Riser Hydrodynamics: Simulation Using Kinetic Theory

Augusto Neri
Consiglio Nazionale delle Ricerche, Centro di Studio per La Geologia Strutturale e Dinámica dell'Appennino, Dip.to di Scienze della Terra, Università di Pisa, Pisa, Italy 52126

Dimitri Gidaspow
Dept. of Chemical and Environmental Engineering, Illinois Institute of Technology, Chicago, IL 60616

Computational fluid dynamics (CFD) for fluidization is reaching maturity (Roco, 1998). It has become common practice to compare time-averaged solid velocities and concentrations to measurements of fluxes and densities. The dynamic behavior of the riser, however, has not been previously compared to experiments. This article shows that the dynamics of solids flow in the riser is in the form of clusters, but the time-averaged particle concentrations and fluxes give us the core-annular flow regime in agreement with measurements. The computed clusters, which are essentially compressible gravity waves, produce major frequencies of density oscillations in agreement with measurements. The model and the CFD code compute granular temperature distributions, agreeing qualitatively with data. For volume fraction around 3–4%, which is the average particle concentration in the riser, the computed viscosity agrees with our experimental measurements.

Introduction

Fluid catalytic cracking (FCC) is a trillion dollar worldwide industrial operation that converts heavy hydrocarbons (petroleum) to lower molecular-weight products, such as gasoline (Avidan, 1997; Squires et al., 1985).The development of very active catalysts allowed the cracking to be completed in short-contact-time riser (vertical-pipe) reactors. Hence the older bubbling-bed reactors were replaced with risers. However, it was only a decade ago that the oil industry using gamma-ray techniques (Sun and Koves, 1998) learned that their large-diameter risers operate in the core-annular flow regime: the core is very dilute. The core-annular structure leads to two main problems: (1) inefficient gas–solids contact, and (2) back mixing due to nonuniform radial distributions (Jin et al., 1997). Figure 12 in the article by Therdthianwong and Gidaspow (1994) shows that the absorption of sulfur dioxide by 210-μm calcined dolomite particles in a riser is much smaller in the dilute core compared to the absorption in the dense core. This unfavorable radial volume fraction distribution of solids in the riser has led to consideration of new schemes of contacting for a refinery of the twenty-first century.

In response to the U.S. Chemical Industry Technology Vision 2020 report, an industry-led Department of Energy, Office of Industrial Technology multiphase fluid-dynamcis research consortium was formed (Thompson, 1999). It consists of six national laboratories and five universities and American chemical companies that support the universities. Its mission is to develop advanced experimental and computational fluid dynamics tools for gas–solid systems. Riser hydrodynamics was reviewed by Jackson (1993) and by Gidaspow (1994). Crowe et al. (1998) reviewed the more dilute flows. The early hydrodynamic models were developed by Davidson (1961), Jackson (1963), and Soo (1967).

The multiphase gas–solid flow in a riser of a circulating fluidized bed (CFB) has been studied both theoretically and experimentally, by numerous research groups. Several experimental studies have been performed to understand the global flow pattern along the riser of a CFB. Capes and Nakamura

Correspondence concerning this article should be addressed to A. Neri: Consiglio Nazionale delle Ricerche, CSGSDA, Dip. to di Scienze della Terra, Università di Pisa, Via S. Maria 53, I-56126 Pisa, Italy.

(1973), Weinstein et al. (1986), Geldart and Rhodes (1986), Bader et al. (1988), Miller and Gidaspow (1992), Martin et al. (1992), and Samuelsberg and Hjertager (1996a) showed a nonhomogeneous distribution of particles along the radial and axial coordinates of the riser. Core-annular flow and cluster formation were found and related to different operating conditions such as mass flux, superficial velocity, and particle diameter.

The hydrodynamics of CFBs has also been investigated by using different modeling approaches. Arastoopour and Gidaspow (1979a,b) established four different two-phase flow models for the description of one-dimensional steady-state pneumatic conveying systems. Rhodes and Geldart (1986) used a semiempirical model based on entrainment and expansion bed correlations to predict axial and radial nonhomogeneous distribution of particles in a CFB. Tsuo and Gidaspow (1990) were the first to simulate cluster formation and predict the core-annular flow of particles by using a two-dimensional transient two-phase flow model, based on a finite difference technique, with a viscosity as an input. Arastoopour et al. (1990) similarly developed a steady-state two-dimensional gas–solid flow model using the method of lines. In both cases, including the studies of Kuipers et al. (1992), Lyczkowsky et al. (1993), and Benyahia et al. (1998a) viscosity values based on experimental measurements were used to model the viscous effects of the solid phase.

In recent years, one step forward in the understanding of gas–solid systems has been taken by the development of kinetic theory for two-phase flows based on the theory for nonuniform dense gases described in Chapman and Cowling (1970). The pioneering paper of Lun et al. (1984) applied the kinetic theory to granular flows. Gidaspow (1994) has reviewed this theory. Sinclair and Jackson (1989) first applied the granular flow model to a fully developed gas–solid flow in a pipe. Ding and Gidaspow (1990)—starting with the Boltzmann integral-differential equation and assuming a Maxwellian frequency distribution for the particle velocity—derived expressions for solid viscosity and pressure of a dense gas–solid flow. Gidaspow (1994) extended the Ding and Gidaspow (1990) formulation to both dilute and dense cases by considering a non-Maxwellian velocity distribution. Such a formulation, in addition to the CFBs, has been applied to the analysis of liquid–solid flows (Gidaspow et al., 1991) and to full-scale CFB loops (Gidaspow et al., 1992).

The kinetic theory of gas–particle flow recently has been verified by laboratory measurements (Gidaspow and Huilin, 1996, 1998). Measurements of granular temperature and solid pressure allowed the determination of particle viscosity for FCC particles. Particular kinematic viscosity was obtained as the product of the mean free path between collisions and the random oscillating particle velocity. Such an estimate agrees well with independent estimates for FCC particles obtained by using pressure-drop/shear data and a Brookfield viscometer. Measurements also show that a relation exists between pressure, temperature, and solid fraction analogous to the ideal gas law, that is, (solid pressure)/(granular temperature $\times$ bulk density) = 1.0.

In the present study, the kinetic-theory approach has been applied to the study of a gas–particle flow of FCC particles in the riser of a CFB. The flow pattern has been investigated by a transient two-dimensional two-phase flow model. The model was used to reproduce two-phase flow experiments performed at Illinois Institute of Technology (IIT) by Miller and Gidaspow (1992). Such experiments have already been the subject of several investigations (Arastoopour and Sue-Kim, 1994; Cao and Ahmadi, 1995; Samuelsberg and Hjertager, 1996a,b; Hjertager et al., 1998) and, in some cases, a good agreement between prediction and data was obtained. The purpose of this study is to extend the comparisons between model prediction and data to recently measured variables such as granular temperature, solid pressure and viscosity, and oscillation frequency. Emphasis here is placed particularly on the effect of the adopted coordinate systems in the computer simulation, inlet geometry, cohesive forces, wall restitution coefficient, as well as on the analysis of the oscillations characterizing the riser dynamics.

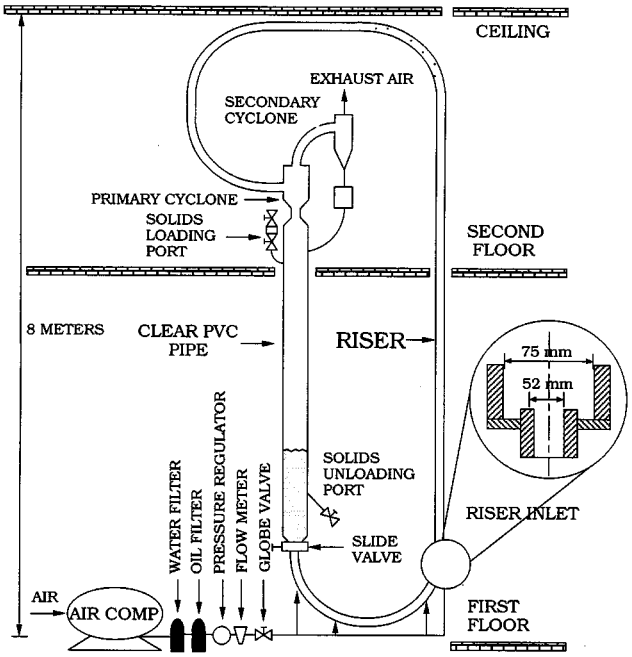

Figure 1. Circulating fluidized bed at IIT.

Modified from Miller and Gidaspow (1992).

Simulation results are able to describe the main features of the gas–solid flow patterns in the riser, such as the core-annular flow regime and the strongly transient behavior of the flow. Agreement between predicted and experimental data are reasonably good and allow us to increase our confidence in the adopted theory and computer code. The experimental setup, governing equations, numerical method, and simulation results are presented in the following sections.

Overview of the Experimental Setup

Figure 1 shows the CFB unit at IIT. Air and particles enter the CFB through the bottom U-tube whose diameter is smaller than that of the riser. Its inner diameter is 5.2 cm. The particle feed rate is controlled by a slide valve. The riser is 7.5 cm in ID and 6.58 m long, and particle size distribution has an average of 75 μm in diameter (Miller, 1991). The outflow stream enters a primary cyclon where the gas–particle

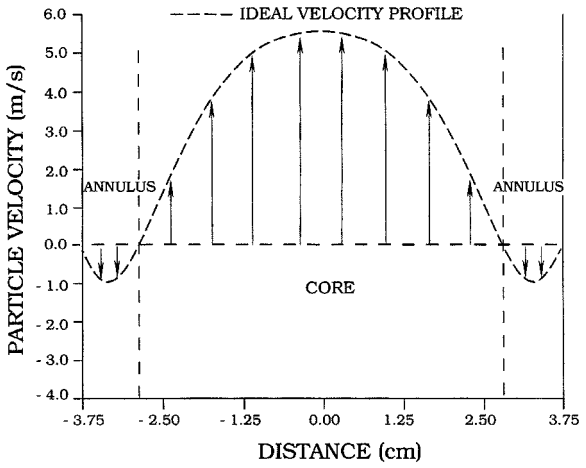

Figure 2. Solid velocity profile for the vertical transport of 75-μm particles along the riser of a CFB.

Modified from Miller and Gidaspow (1992).

separation process mainly occurs. Additional separation is performed in the secondary cyclon. Particles are recycled to a storage PVC hopper.

Several measurements were performed by Miller and Gidaspow (1992) at different points and sections of the riser, pointing out large nonuniformities in mass flux, velocity, and solid volumetric fraction. Time-averaged radial solid-volume fractions were obtained with an X-ray densitometer. Fluxes were determined by an extraction probe, whereas solid velocity was computed indirectly from flux and volumetric fraction data. Experiments were carried out with various gas–particle loading ratios and superficial velocities in order to study the effect of different operating conditions on the two-phase flow hydrodynamics. Figure 2 illustrates the time-averaged vertical solid-velocity profile vs. the radial coordinate of the riser as given by the measurements. The core-annulus flow consists of a low-density central region (core), in which particles are carried up by the gas, and a high-density annular region (annulus) where particles descend along the wall. The core is thinner at the bottom of the riser where we have a high downflow and recycling of particles. Along the riser particles move mainly from the core to the wall where they accumulate and descend. We refer to Miller and Gidaspow (1992) for a more complete description of the system and dynamics. However, it is important to highlight that the flow is strongly transient and oscillates with a characteristic frequency. Gidaspow et al. (1995) studied the dynamics of the flow by measuring density oscillations in the developed regions and in the entrance regions of the riser for operating conditions similar to those adopted by Miller and Gidaspow (1992).

Kinetic-Theory-Based Flow Model

The model adopted is based on the fundamental concept of interpenetrating continua for multiphase mixtures. According to this theory different phases can be present at the same time in the same computational volume. Such an idea is made possible by the introduction of a new dependent variable, the volume fraction, ϵ_i, of each phase i. The fundamental equations of mass, momentum, and energy conservation are then solved for each considered phase. Appropriate constitutive equations have to be specified in order to describe the physical and rheological properties of each phase and to close the conservation equations. In this model, solid viscosity and pressure are derived by considering the random fluctuation of solid velocity and its variations due to particle–particle collisions and the actual flow field. Such a random kinetic energy, or granular temperature, can be predicted by solving, in addition to the mass and momentum equations, a fluctuating kinetic energy equation for the particles. The solid viscosity and pressure can then be computed as a function of granular temperature at any time and position. Particles are considered smooth, spherical, inelastic, and undergoing binary collisions. The adoption of the second approximation distribution function allows us to apply the theory to both dense and dilute two-phase flows. Finally, gas-pressure gradients do not appear in the solid equation, according to model B of Gidaspow (1994). A more complete discussion of the implemented kinetic theory model and the derivation of the solid rheological properties can be found in Gidaspow (1994) and Neri (1998). In the following subsections, governing equations, boundary, and initial conditions, as well as the numerical procedure, are described.

Governing equations

Continuity Equations

$$\frac{\partial}{\partial t}(\epsilon_g \rho_g) + \nabla\cdot(\epsilon_g \rho_g \boldsymbol{v}_g) = 0 \tag{1}$$

$$\frac{\partial}{\partial t}(\epsilon_s \rho_s) + \nabla\cdot(\epsilon_s \rho_s \boldsymbol{v}_s) = 0. \tag{2}$$

Momentum Equations

$$\frac{\partial}{\partial t}(\epsilon_g \rho_g \boldsymbol{v}_g) + \nabla\cdot(\epsilon_g \rho_g \boldsymbol{v}_g \boldsymbol{v}_g) = -\nabla P_g + \nabla T_g + \rho_g g + \beta(\boldsymbol{v}_s - \boldsymbol{v}_g) \tag{3}$$

$$\frac{\partial}{\partial t}(\epsilon_s \rho_s \boldsymbol{v}_s) + \nabla\cdot(\epsilon_s \rho_s \boldsymbol{v}_s \boldsymbol{v}_s) = \nabla T_s + \epsilon_s(\rho_s - \rho_g) g - \beta(\boldsymbol{v}_s - \boldsymbol{v}_g) \tag{4}$$

Fluctuating Energy Equation for the Solid

$$\frac{3}{2}\left[\frac{\partial}{\partial t}\epsilon_s \rho_s \Theta + \nabla\cdot(\epsilon_s \rho_s \boldsymbol{v}_s \Theta)\right] = T_s{:}\nabla \boldsymbol{v}_s + \nabla\cdot\kappa\nabla\Theta - \gamma. \tag{5}$$

Constitutive Equations. The equation of state of the gas was assumed to be the ideal gas law:

$$P_g = \rho_g \tilde{R} T_g, \tag{6}$$

whereas the solid phase was considered incompressible.

The gas phase was modeled as a compressible Newtonian fluid, and no turbulence viscosity model was used. The stress tensor can be represented as

$$T_g = 2\epsilon_g \mu_g \tau_g, \tag{7}$$

with

$$\tau_g = \frac{1}{2}\left[\nabla v_g + (\nabla \mathbf{v}_g)^T\right] - \frac{1}{3}(\nabla \cdot v_g) I \tag{8}$$

The solid stress tensor, T_s, can be expressed in terms of the solid pressure, P_s, bulk solid viscosity, ξ_s, and shear solid viscosities, μ_s, as

$$T_s = (-P_s + \xi_s \nabla \cdot v_s) I + 2\mu_s \tau_s, \tag{9}$$

with

$$\tau_s = \frac{1}{2}\left[\nabla v_s + (\nabla v_s)^T\right] - \frac{1}{3}(\nabla \cdot v_s) I. \tag{10}$$

These solid properties can be determined as a function of granular temperature according to the following relations:

$$P_s = \epsilon_s \rho_s \Theta\left[1 + 2(1+e) g_0 \epsilon_s\right] \tag{11}$$

$$\xi_s = \frac{4}{3}\epsilon_s^2 \rho_s d_s (1+e) g_0 \left(\frac{\Theta}{\pi}\right)^{1/2} \tag{12}$$

$$\mu_s = \frac{2\mu_{s,\mathrm{dil}}}{(1+e) g_0}\left[1 + \frac{4}{5}(1+e) g_0 \epsilon_s\right]^2 + \frac{4}{5}\epsilon_s^2 \rho_s d_s (1+e) g_0 \left(\frac{\Theta}{\pi}\right)^{1/2}, \tag{13}$$

where $\mu_{s,\mathrm{dil}}$ is the dilute solid viscosity and g_0 is the radial-distribution function expressing the statistics of the spatial arrangement of particles. In this study the following expressions were adopted:

$$\mu_{s,\mathrm{dil}} = \frac{5\sqrt{\pi}}{96}\rho_s d_s \Theta^{1/2} \tag{14}$$

$$g_0 = \left[1 - \left(\frac{\epsilon_s}{\epsilon_{s,\max}}\right)^{1/3}\right]^{-1} \tag{15}$$

Recently, Gidaspow and Huilin (1998) showed that this form of the radial distribution function agrees with experimental data for FCC particles. Furthermore, in order to solve the fluctuating energy equation, we need to specify the conductivity of the particle fluctuating energy, κ, and the collisional rate of energy dissipation per unit volume, γ:

$$\kappa = \frac{2\kappa_{\mathrm{dil}}}{(1+e) g_0}\left[1 + \frac{6}{5}(1+e) g_0 \epsilon_s\right]^2 + 2\epsilon_s^2 \rho_s d_s (1+e) g_0 \left(\frac{\Theta}{\pi}\right)^{1/2}, \tag{16}$$

with

$$\kappa_{\mathrm{dil}} = \frac{75\sqrt{\pi}}{384}\rho_s d_s \Theta^{1/2}, \tag{17}$$

$$\gamma = 3(1-e^2)\epsilon_s^2 \rho_s g_0 \Theta\left[\frac{4}{d_s}\left(\frac{\Theta}{\pi}\right)^{1/2} - \nabla \cdot v_s\right]. \tag{18}$$

It should be noted that, in the kinetic energy balance adopted, the effect of energy production due to gas turbulence has been balanced by the energy dissipation term representative of the fluid drag. Such an assumption appears reasonable in the light of the results obtained by Ahmadi and Ma (1990) and Cao and Ahmadi (1995), who derived and solved a kinetic-energy equation for the gas phase for steady developed flow. Here we thus assume that the gas oscillates the same as the particles. Hence we do not need the fluctuating energy equation for the gas.

Finally, we need to specify the gas–solid drag coefficient for different solid concentrations (Gidaspow, 1994).

For $\epsilon_g \geq 0.8$:

$$\beta = \frac{3}{4} C_d \frac{\epsilon_s \rho_g |v_g - v_s|}{d_s} \epsilon_g^{-2.65}, \tag{19}$$

where the drag coefficient C_d is given by

$$C_d = \frac{24}{Re_s}\left(1 + 0.15 Re_s^{0.687}\right); \quad Re_s < 1{,}000$$
$$= 0.44; \quad Re_s \geq 1{,}000 \tag{20}$$

$$Re_s = \frac{\epsilon_g \rho_g d_s |v_g - v_s|}{\mu_g}. \tag{21}$$

For $\epsilon_g < 0.8$,

$$\beta = 150\frac{\epsilon_s^2 \mu_g}{\epsilon_g^2 d_p^2} + 1.75\frac{\rho_g \epsilon_s |v_g - v_s|}{d_s \epsilon_g}. \tag{22}$$

Initial and boundary conditions

The definition of appropriate initial and boundary conditions is critical for the carrying out of a realistic simulation. As far as inlet conditions are concerned, several different flow conditions were implemented and used in the simulations. Some of them assume uniform plug-flow velocity and solid concentration profile on the entire base area of the riser. Some others assume a uniform or a trapezoidal profile only on the circular area of the inner tube (see Figure 1). The latter conditions are actually closer to the real inlet feeding conditions, while the former are a poor approximation. In the following, the effect of two different inlet conditions, with feeding through an inner circular area at the riser base, will be illustrated. Solid velocity, volume fraction, and granular temperatures at the inlet of the riser were measured (Gidaspow et al., 1997).

As far as the outlet flow conditions are concerned, the system geometry has been changed since there are no practical

outlet conditions. An attempt to model the horizontal section showed that it requires several months of computer time. As a consequence, the smooth bend at the top of the riser has been modeled as a 90° bend. Different locations and sizes of the outlet cell produced appreciable effects, mainly in the upper part of the riser, but were unable to change the global pattern of the flow illustrated in the following sections. Furthermore, a free-outflow condition was assumed at the outlet cell.

Particularly important is also the specification of appropriate boundary conditions at the walls. For the gas a no-slip boundary condition was used. For the solid we used the Johnson and Jackson (1987) slip boundary condition given by their Eq. 2.10 with zero friction, as shown below:

$$u_{s,w} = -A\frac{\partial u_{s,w}}{\partial n}, \tag{23}$$

where the slip coefficient A is expressed in terms of a specularity coefficient Φ, as

$$A = \frac{6\mu_s \epsilon_{s,\max}}{\sqrt{3}\,\pi\Phi\rho_s\epsilon_s g_0\sqrt{\Theta}}. \tag{24}$$

Hui et al. (1984) derived a primitive form of this balance using intuitive arguments. The specularity coefficient is the fraction of total momentum transferred to the wall when particle collides with it and it represents a measure of wall roughness.

For the granular temperature wall boundary condition the Johnson and Jackson (1987) Eq. 2.13 was used. It is obtained by equating the granular flux to collisional dissipation at the wall with a correction for slip, as given below:

$$\Theta_w = -B_1\frac{\partial\Theta_w}{\partial n} + B_2 \tag{25}$$

$$B_1 = \frac{\kappa\Theta}{\gamma_w}; \qquad B_2 = \frac{\sqrt{3}\,\pi\Phi\rho_s\epsilon_s u_{s,\text{slip}}^2 g_0\Theta^{3/2}}{6\epsilon_{s,\max}\gamma_w}. \tag{26}$$

The dissipation is expressed in terms of a wall restitution coefficient that was measured under dilute conditions by Gidaspow and Huilin (1998), as given below:

$$\gamma_w = \frac{\sqrt{3}\,\pi\left(1-e_w^2\right)\epsilon_s\rho_s g_0\Theta^{3/2}}{4\epsilon_{s,\max}}. \tag{27}$$

In order to assess the effect of boundary conditions at the wall, two cases with a different restitution coefficient of the wall also have been investigated and will be described in the next subsection. Finally, due to the low value and uncertainty associated with the specularity coefficient, Φ, a slip condition for the solid at the wall was a good approximation and has been adopted in the presented simulations. When a symmetrical condition is imposed at the riser axis or middle plane, a zero gradient condition for all variables was used along the axis.

As an initial condition, we assumed an empty riser at a uniform pressure. As a consequence, during the first 20 s, the riser becomes denser and denser until quasi-steady-state conditions are reached for the time-averaged outlet flux. Time-averaged distributions of flow variables are computed starting from this time and typically cover a period of 20–50 s.

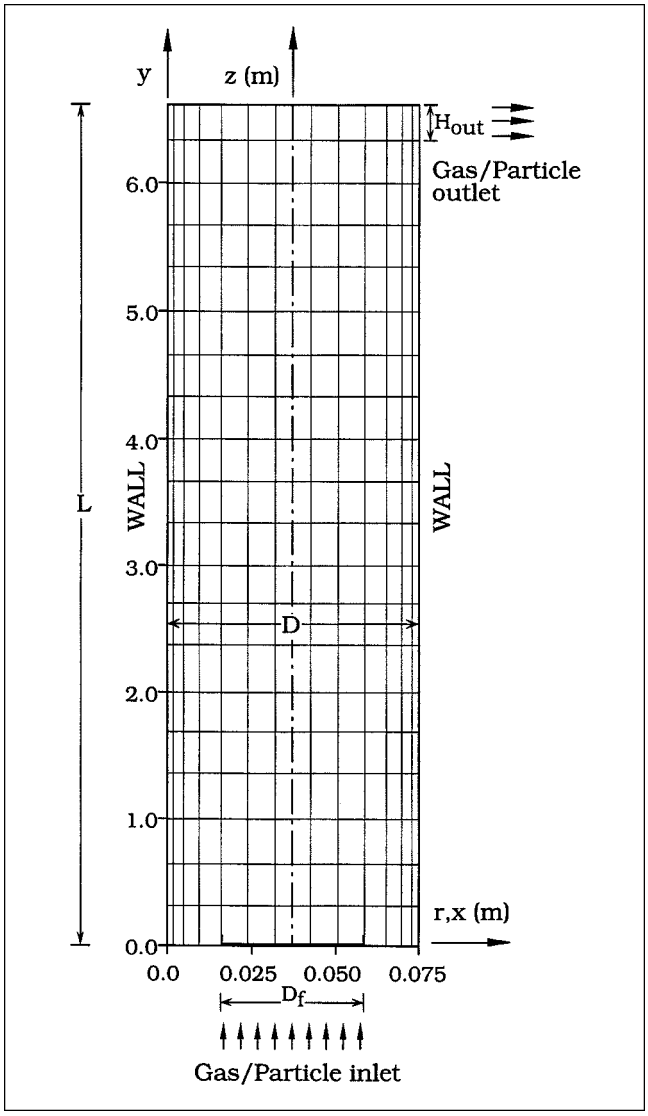

Figure 3. Computational domain and coordinate systems adopted in the simulations.

Coordinate systems and solution procedure

The solution of the preceding conservation equations depends on the boundary and initial conditions adopted, as well as on the coordinate system. Figure 3 illustrates the two-dimensional computational domain and coordinate systems used in the simulations. Both two-dimensional Cartesian (x,y) and cylindrical (r,z) coordinates have been applied for the description of the riser. With Cartesian coordinates, simulations have been performed assuming both symmetry and no symmetry conditions with respect to the axis of the riser. With symmetry only one half of the riser has been described. Uniform and nonuniform grids of different sizes were also used (Neri, 1998). It the following pages, results that pertain to

Table 1. System Geometry, Physical Properties, and Operating Conditions Employed in Simulation CFB-1.

Property/Parameter	Value
L (m)	6.58
D (m)	0.075
D_f (m)	0.0525
H_{out} (m)	0.03
d_s (μm)	75
ρ_s (kg/m^3)	1654
e	0.999
e_w	0.96
μ_g (Pa·s)	1.8×10^{-5}
$\epsilon_{s,in}$	0.005
Θ_{in} (m/s)^2	0.6
$P_{g,in}$ (kPa)	118.6
$W_{s,in}$ (kg/m^2·s)	20.4
$u_{g,in}$ (m/s)	2.61

just one optimal grid will be presented. Such an optimal grid was shown to properly represent the flow hydrodynamics and, at the same time, to optimize computer time. For this grid cell sizes are uniform in both coordinate systems and are equal to 0.375 cm in the r/x direction and 4.84 cm in the y/z direction. Only the size of the upper cell row has been varied to accommodate the size of the outlet cell, H_{out}.

The solution of the hydrodynamic equations was obtained by their discretization on a computational grid and by the adoption of a finite difference Eulerian method, known as the implicit multifield (IMF) method (Harlow and Amsden, 1975). The IMF method was demonstrated to be useful in the description of a wide variety of multiphase problems (Gidaspow, 1994). According to this method the various phases are treated as interpenetrating continua, and the continuum differential equations are solved for each phase. Scalar quantities are computed at the cell center, whereas velocity components are computed on a staggered grid coinciding with the cell boundaries. A donor-cell method was adopted. Numerical solution is reached by an iterative algorithm for pressure. The solution method treats the pressure and drag terms implicitly, whereas convective, viscous, and gravitational terms are considered explicitly in the momentum equations. Because of the non-fully implicit time differencing, the Courant stability criterion limits the time step size in each computational cycle. Available computer resources also impose a limitation on the number of cells, and therefore on cell size. Very small cells provide more accurate results but demand a large number of cells and very small time steps, which, in turn, require very long computing times. In the present study, different grid sizes, time steps, mass residuals, and convergence parameters were employed. The computer code developed derives from Los Alamos K-FIX code (Rivard and Torrey, 1977) and has been improved by the addition of several features such as the just described kinetic-theory equations (Gidaspow, 1994). The code is also similar

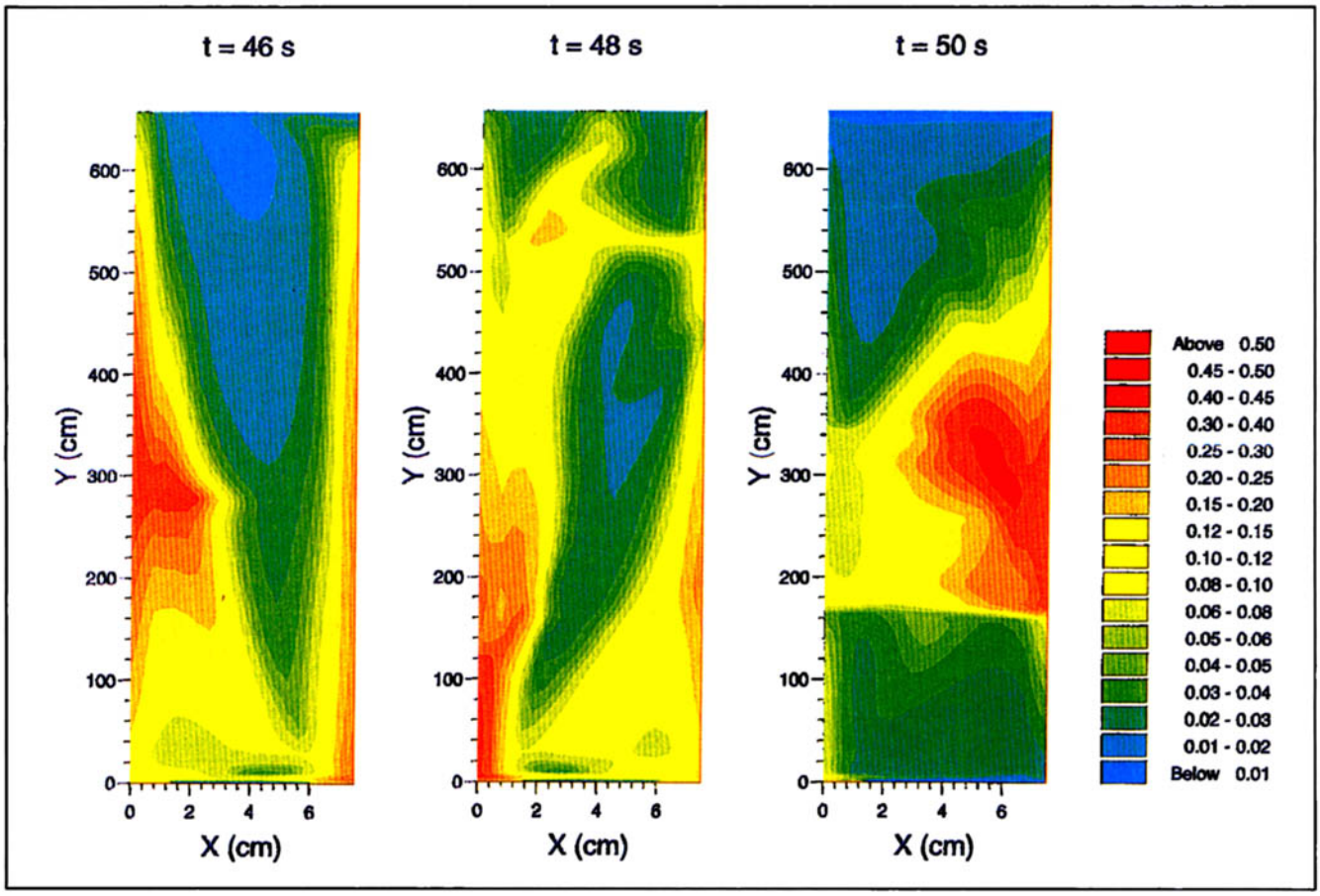

Figure 4. Distribution of solid volumetric fraction for Simulation CFB-1 at 46, 48, and 50 s.

to the M-FIX code developed at Morgantown Energy Technology Center (Syamlal et al., 1993).

Simulation Results

Several simulations have been performed in order to investigate the effect of different operating conditions, model assumptions, and to get an adequate description of the observed two-phase flow pattern in the riser of the CFB. Most of the results reported below pertain to the same operating conditions, but similar considerations can be done for the other cases performed. Some simulations, in particular, have been performed by using both Cartesian and cylindrical coordinates in order to assess the effect of such hypotheses. In the following paragraphs, results pertaining to Cartesian coordinates, with and without symmetry with respect to the axis of the riser, will be presented. When symmetry is imposed as a left boundary condition, similar results also are obtained with cylindrical coordinates. All simulations are continued for 50 s of real simulation time. Time-averaged distribution of variables is then computed considering the last 30 s of simulation. In the following subsections, simulation results are presented and compared to the measurements by Miller and Gidaspow (1992), Gidaspow et al. (1995), and Gidaspow and Huilin (1996, 1998).

Reference simulation (Simulation CFB-1)

Table 1 summarizes the system geometry, physical properties, and operating conditions employed in Simulation CFB-1. Inlet flow is considered through a circular area of diameter D_f and assumes a uniform velocity profile (plug flow) for the gas and solid particles. Due to such an inlet geometry, the feed solid flux has been corrected by the ratio between the circular areas of the two cross-sections. Inlet solid volumetric fraction, granular temperature, and solid velocity have been measured directly (Gidaspow et al., 1997). The outlet geometry is represented by a single 3.0 cm cell located on the right-hand-side wall at the top of the riser. A constant restitution coefficient of 0.999 has been assumed for particle−particle collisions, whereas a value of 0.96 has been used between particles and the plastic wall according to the measured value in the dilute regime (Gidaspow and Huilin, 1998).

The simulation was performed adopting Cartesian coordinates and modeling the entire riser. Due to this approximation, we performed different simulations, keeping either the solid flux in the feed section or the solid flux inside the riser constant. The two recalculated fluxes differ by about 30%. In the following, results obtained keeping constant the solid flux in the feed section are presented even though similar results are obtained for the other case. The main difference is that

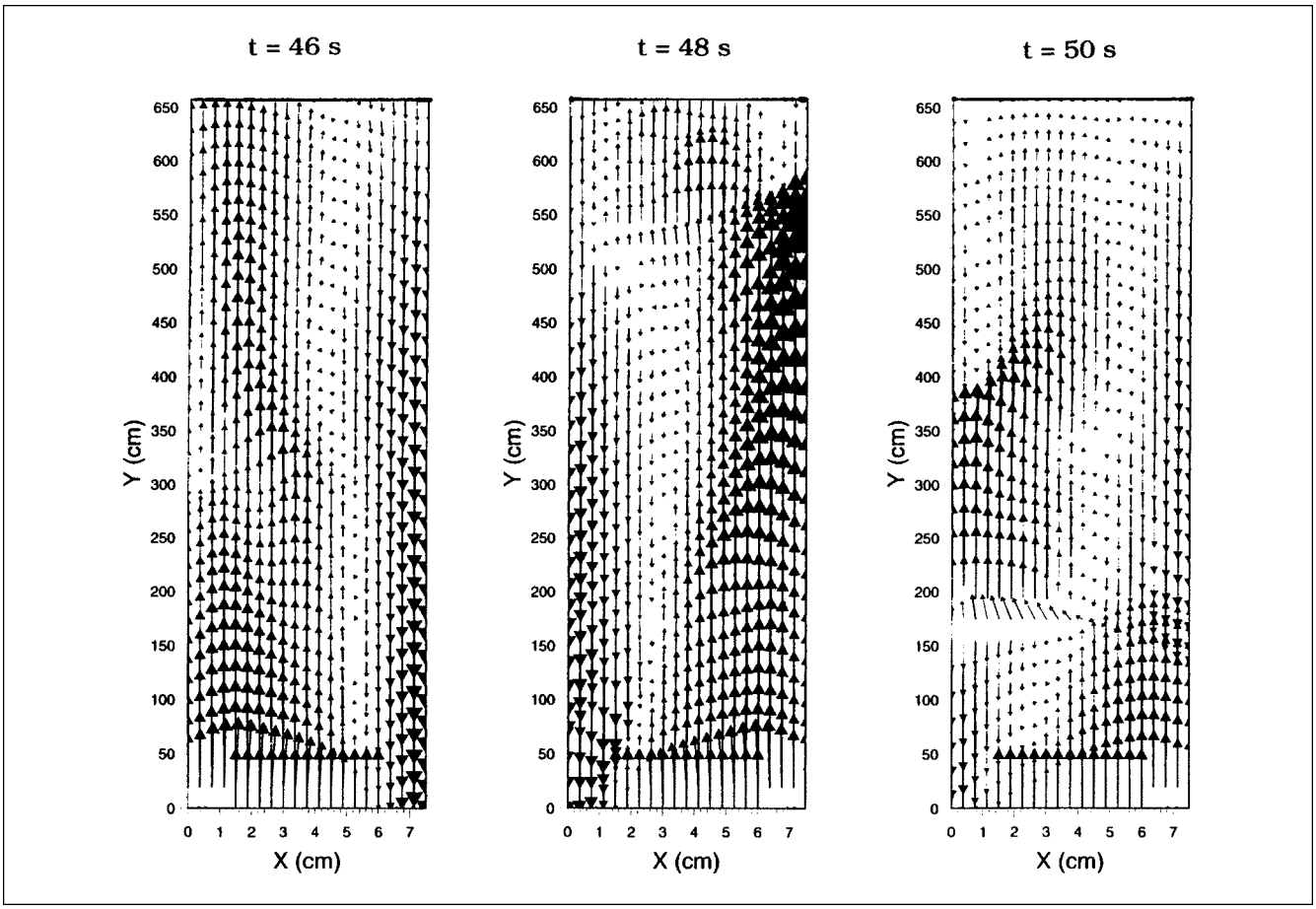

Figure 5. Solid velocity field for Simulation CFB-1 at 46, 48, and 50 s.

The inlet velocity is about 5 m/s, and the maximum velocity at 48 s is about 10 m/s.

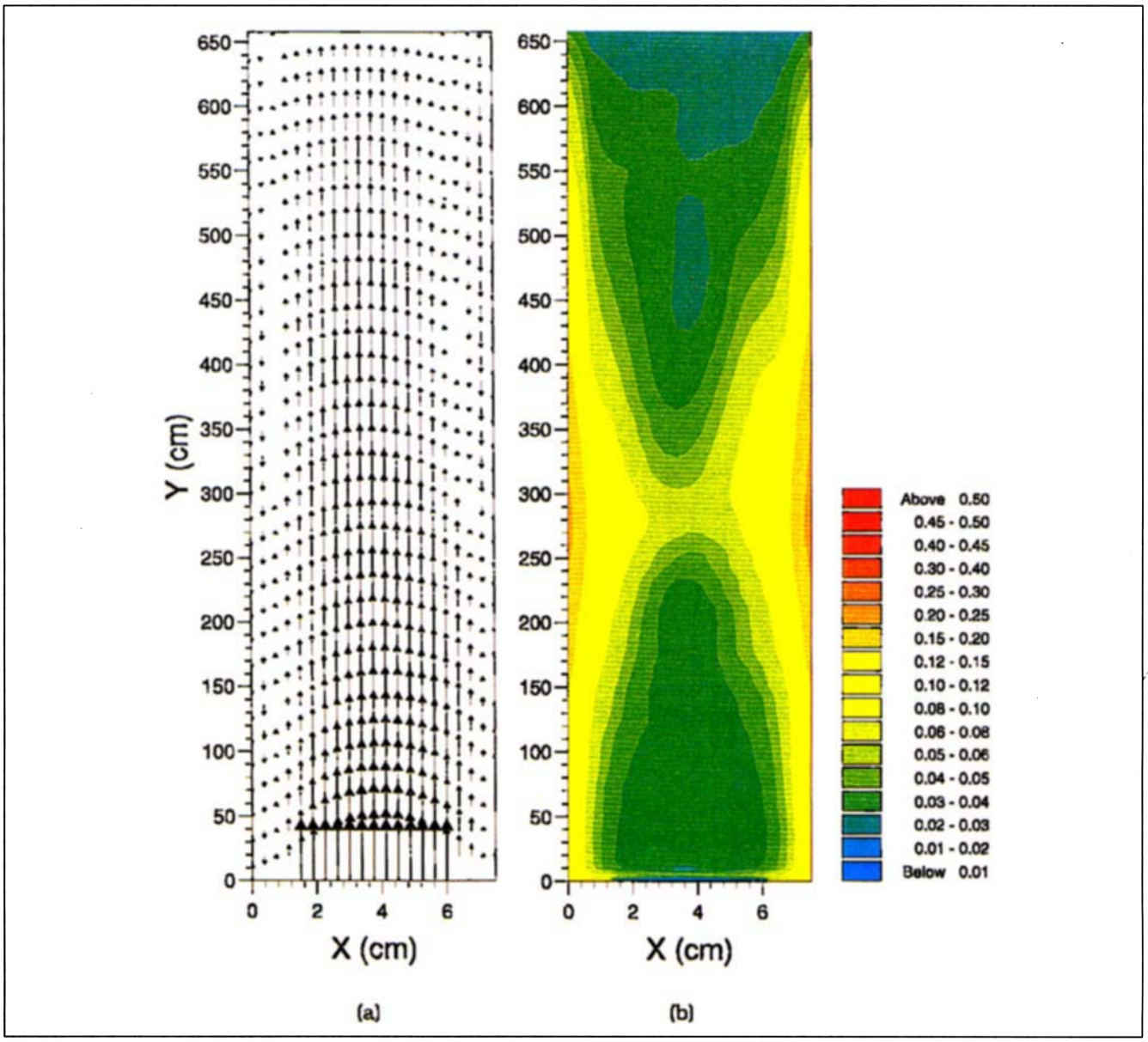

Figure 6. Time-averaged distribution of (a) solid velocity (inlet velocity is 5 m/s) and (b) solid volumetric fraction for Simulation CFB-1.

in the high-flux case core-annular flow-regime conditions are reached in a shorter time.

After an initial period of about 20 s, during which the system becomes denser and denser, the flow hydrodynamics along the riser reaches a regime characterized by a strong nonstationarity. The behavior of the flow is characterized by a periodic formation of particle clusters at the wall. Such dense portions of solid undergo a vigorous up and down motion, thus favoring a strong particle recirculation all over the riser. Such behavior is clearly described in Figures 4 and 5, where the solid volumetric fraction and velocity field are reported, respectively. Distributions refer to three different times—46, 48, and 50 s—from the beginning of the simulation. The strong nonhomogeneities of the flow density as well as the complex and transient velocity field are evident. It should be noted how downflow conditions at one wall are mostly associated with an upflow condition at the other wall, but more complex combinations are possible, too. In particular, upward or downward velocities up to 10 m/s are reported at some instants (see 48 s in Figure 5). Upflow and downflow are not necessarily associated with the low and high density of the flow, respectively, but different situations can occur as well. A characteristic feature of the flow, as better described below, is the oscillating motion of solid clusters from one wall to the other through the center line of the riser.

In order to compare simulation results with Miller and Gidaspow's (1992) data, time-averaged distributions of flow variables have been computed. Figure 6 shows the time-averaged distribution of solid velocity field (Figure 6a), and solid volumetric fraction (Figure 6b), over the time period 20–50 s.

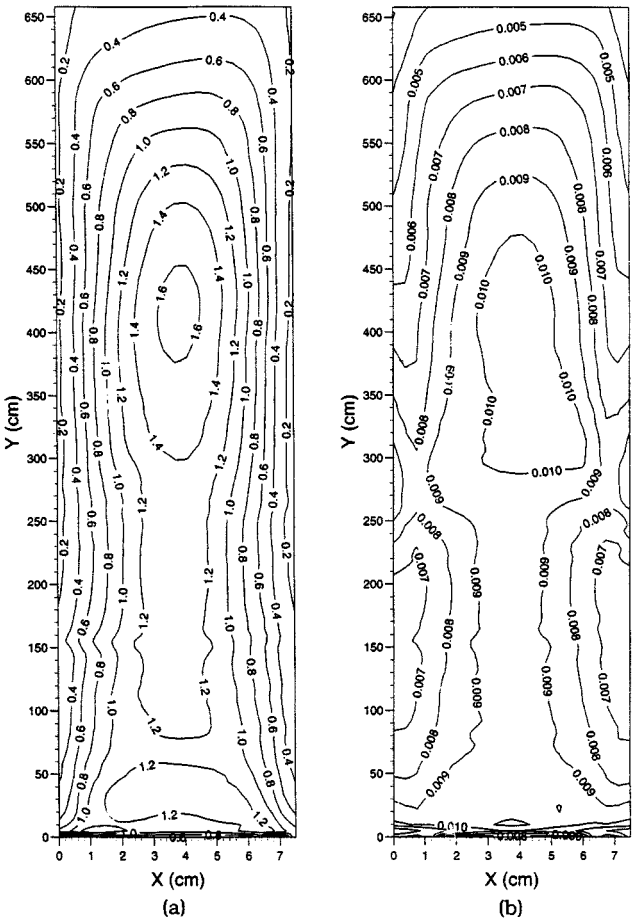

Figure 7. Time-averaged distribution of (a) granular temperature $(m/s)^2$, and (b) solid viscosity (Pa·s) for Simulation CFB-1.

The two distributions clearly illustrate the core-annular pattern of the flow. The solid mainly accumulates and moves downward at the wall, whereas a dilute gas–solid stream flows upward in the core of the riser. The lower region of the riser is denser than the upper-dilute region even though the solid mainly accumulates at the walls in both regions. In detail, the highest values of solid volumetric fraction are equal to about 0.25 and are observed at about 2.5 m from the riser bottom. In such a portion of the riser, the strong upward and downward motion of the clusters is particularly effective in causing them to stay in this region. It is also interesting to observe how the time-averaged distribution of the flow pattern is almost axisymmetric with respect to the riser axis despite the unsymmetric configuration of the outlet geometry. In the lower portion of the riser, only a slightly larger downflow is observed at the lefthand-side wall, whereas, in the upper part, maximum downflow is observed just below the outlet cell.

The time-averaged distributions of granular temperature and solid viscosity are reported in Figure 7. Figure 7a shows that the central dilute region of the riser is characterized by higher values of granular temperature with respect to the dense wall region. Maximum values are reached in the central upper region of the riser where the flow is more dilute and shear effects seem to be greater. As discussed below, such behavior can be easily argued from the kinetic-theory equations given earlier, and appears to be consistent with experimental observations (Gidaspow, 1994; Gidaspow and Huilin, 1996). Figure 7b shows the solid shear viscosity distribution. As observed for granular temperature, large values are reported in the core region, even though the whole distribution seems quite uniform.

A more direct comparison between simulation results and experimental data was obtained by plotting the radial profile of some measured variables. Three sections, at 1.86, 4.18, and 5.52 m above the flow distributor, have been investigated. Figure 8 shows comparisons between experimental and predicted solid volume fraction, solid axial velocity, and solid flux across these three sections. Predicted profiles refer again to time-averaged values over the period 20–50 s. As we can see from the diagrams, the model is able to describe quantitatively the accumulation of solid at the wall for all of the three sections. Core solid concentrations also appear fairly similar at the riser axis, even though data show a profile that is quite a bit flatter. As regards the axial solid velocity, the comparison is less satisfactory overall. At the lower section, maximum velocity is predicted with good approximation, whereas the downflow is underestimated along both walls. As far as the middle and upper sections are concerned, the situation is reversed, with a good agreement on the downflow velocity, but with a relevant underestimation of about 2 m/s of the core upward velocity. It should be noted, however, that the underestimation of the solid velocity is partially compensated for by the overestimation of the solid fraction, resulting in a good agreement between data and predictions of the solid fluxes.

Figure 9 shows the time-averaged radial profiles of the granular temperature, solid viscosity, and solid pressure as computed by the kinetic theory model, across the three sections reported earlier. As we can see from the reported profiles, the core region appears characterized by granular temperatures and, to a less extent, viscosities greater than those observed in the dense annular region. It is also interesting to note the almost uniform radial distribution of solid pressure across the riser. For all these variables experimental radial profiles are not available and a comparison can only be made at a distance of about 0.5–1 cm from the wall. A reasonable agreement between predicted values and data can be observed for granular temperature (Gidaspow and Huilin, 1996). Values between 1.5 and 2.0 $(m/s)^2$, in particular, have been measured at about 1 cm from the wall and in the dilute portion of the riser for similar operating conditions (Gidaspow and Huilin, 1996, 1998). As regards the solid viscosity, the value of about 0.01 Pa·s obtained by Miller and Gidaspow (1992) also appears to be in good agreement with the predicted value of 0.005–0.008 Pa·s. Furthermore, the existence of a flow region in which the viscosity does not vary very much with changes in radial position, is confirmed by the model results. Finally, solid pressures of about 100 Pa were measured for operating conditions similar to the ones employed in the simulation (Gidaspow and Huilin, 1998).

A further comparison between predicted results and observed data is reported in Figures 10 and 11. Figure 10 shows the behavior of granular temperature in any cell of the riser, as a function of solid volume fraction, at 48 s. The box included illustrates the same dependence as results from previ-

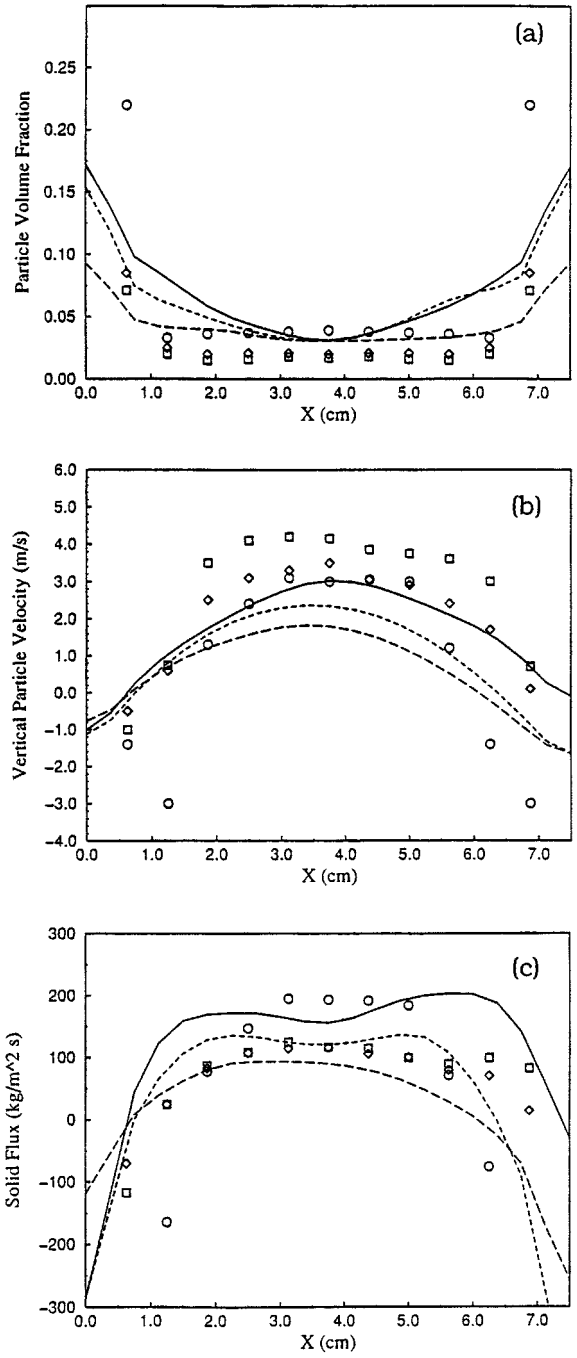

Figure 8. Radial profiles of computed and experimental (a) particle volumetric fraction, (b) particle vertical velocity, and (c) solid flux at 1.86 m (solid line and circles), 4.18 m (short-dashed line and squares), and 5.52 m (long-dashed line and diamonds) above the flow distributor for Simulation CFB-1.

Curves refer to model prediction, symbols to data.

ous experimental work. Similar plots can be computed at different times, but are not reported here for the sake of brevity (Neri, 1998). The diagram clearly shows that the relation between granular temperature and solid volume fraction is not univocal and that it actually depends on Eq. 5. However, as emerges from the comparison with the box included, the diagram presents some interesting features that confirm the experimental evidence. First, the granular temperature exhibits a maximum near a solid volume fraction of about 0.03–0.1. A similar maximum is expected at a solid volume fraction of

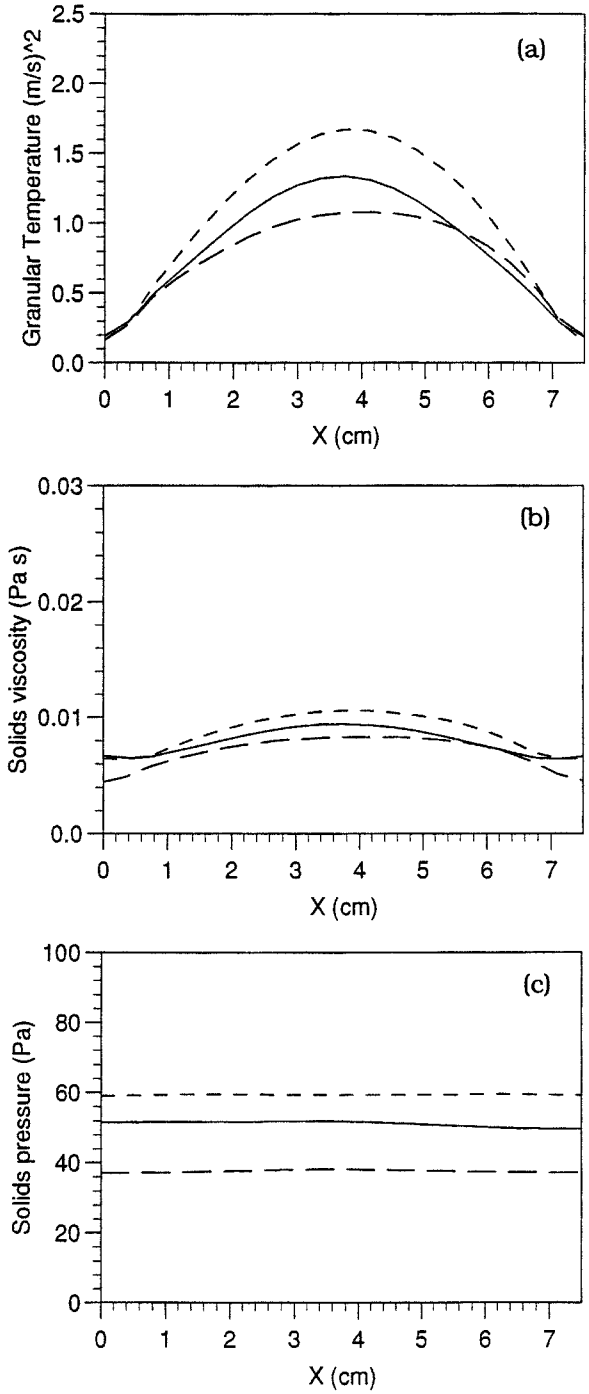

Figure 9. Radial profiles of computed (a) granular temperature, (b) solid viscosity, and (c) solid pressure at 1.86 (solid line), 4.18 (short-dashed line), and 5.52 m (long-dashed line) for Simulation CFB-1.

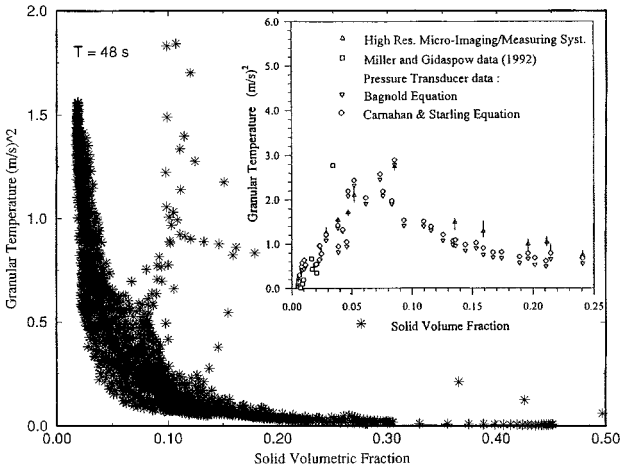

Figure 10. Granular temperature as a function of solid volume fraction at 48 s in any cell of the computational domain for Simulation CFB-1.

The box shows experimental or theoretical granular temperature values. (From Gidaspow and Huilin, 1998.)

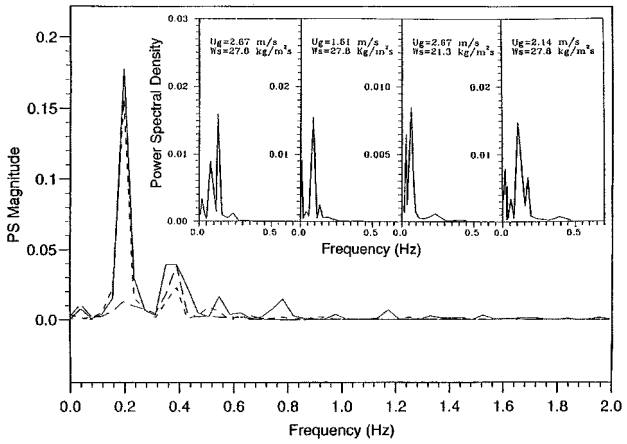

Figure 12. Power spectrum of computed porosity at 0 (solid line), 1.86 (short-dashed line), and 4.18 m (long-dashed line) above the riser inlet on the righthand side wall for Simulation CFB-1.

The box illustrates power spectrum density diagrams of porosity oscillations with similar operating conditions (Gidaspow et al., 1995).

about 0.05−0.1 based on measurements at the wall (Gidaspow and Huilin, 1998). Moreover, granular temperature tends to decrease with the increase in solid volume fraction. Finally, the granular temperature appears to decrease for solid volume concentration decreasing to zero. This behavior is even clearer at different time instants reported in Neri (1998). Such a dependence in the dilute limit was recently proved by Gidaspow and Huilin (1998). A similar behavior of the granular temperature vs. solid fraction is also described by Benyahia et al. (1998b) in the simulation of the PSRI Challenge Problem (Knowlton, 1995).

Figure 11 similarly investigates the dependence of the solid viscosity on the solid volume fraction. A comparison is made between values computed all over the riser and an empirical correlation obtained from data at the wall (Gidaspow et al., 1997). Again in this case, the relation between the two variables is not univocal and points appear quite dispersed. However, the two sets of data compare reasonably well at solid volume fraction below 0.05, whereas above this value a good agreement is observed only for some cells along the wall where clusters move faster. However, both experimental and theoretical estimates exhibit the same trend as a function of solid concentration.

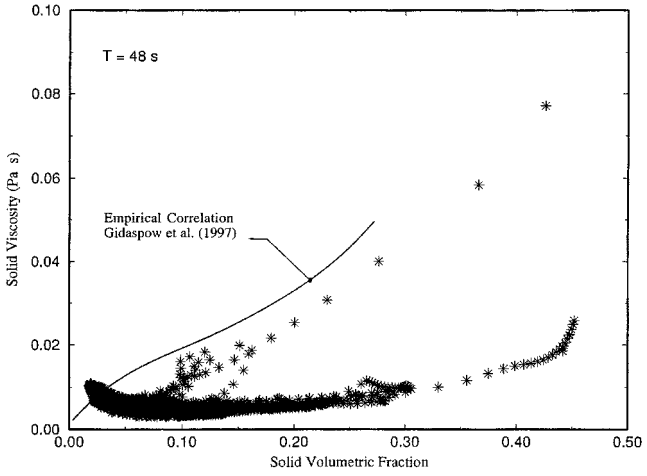

Figure 11. Solid viscosity as a function of solid volume fraction at 48 s in any cell of the computational domain for Simulation CFB-1.

The curve represents the experimental correlation reported by Gidaspow et al. (1997).

Another comparison between simulation results and experimental data has been carried out regarding the analysis of the flow frequencies. Figure 12 shows the power spectrum of porosity oscillations computed at three points located at 0, 1.86, and 4.18 m from the bottom of the riser along the right-hand-side wall. The diagram highlights a major frequency at about 0.2 Hz and a smaller peak at 0.4 Hz. Such estimates are in good agreement with the power-spectrum diagrams shown in the box and measured at similar locations and with similar operating conditions (Gidaspow et al., 1995). Similar estimates also have been reported by Huilin et al. (1997) for pressure oscillations of dense-phase flows of FCC particles.

Axisymmetric representation (Simulation CFB-2)

This simulation investigates the effect of imposing a symmetric boundary condition along the riser axis. The simulation is still performed in Cartesian coordinates and just one half of the riser is simulated. All physical parameters and operating conditions, as well as computational parameters, are the same as Simulation CFB-1. Figure 13 shows the time-averaged solid-particle distribution of Simulation CFB-2. From the comparison of this figure with Figure 6b it clearly emerges that the flow patterns of the two simulations are quite different.

In Simulation CFB-2 the solid mainly accumulates at the top of the riser and no dense region is observed at the riser bottom. More precisely, solid accumulates not only at the riser wall close to the exit cell but also along the symmetry axis. In

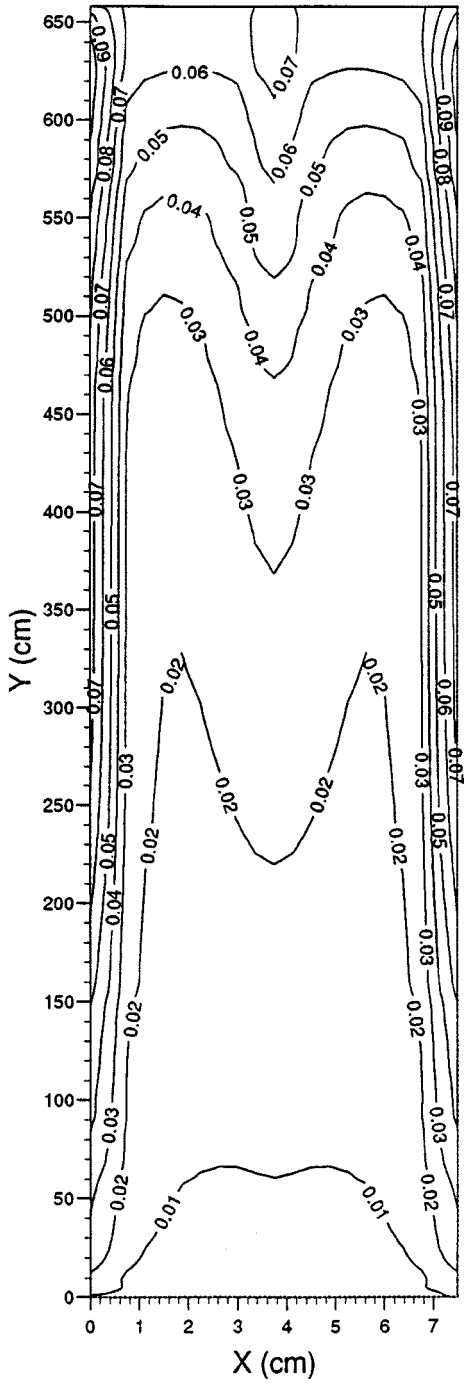

Figure 13. Time-averaged distribution of solid volumetric fraction for Simulation CFB-2.

this case, too, it is possible to observe the formation of clusters of particles moving downward along the wall. In no cases, however, are the clusters able to reach the bottom of the riser; also their formation frequency appears considerably lower than that observed for Simulation CFB-1.

The quite different behavior of Simulation CFB-2 can be associated with the presence of the symmetry axis which, acting as a mirror, does not allow any mass transfer from one wall to the other. Recirculation of material between the two walls is in fact very effective in Simulation CFB-1 and seems to help the formation of quite dense clusters of particles. A similar effect of the symmetry axis also seems to be consistent with results obtained by other investigators who adopted such a description for similar operating conditions (Sinclair and Jackson, 1989; Arastoopour and Sue-Kim, 1994).

Influence of inlet conditions (Simulation CFB-3)

Simulation CFB-3 investigates the effect of a different inlet condition. As mentioned by Miller and Gidaspow (1992), exact inlet conditions are difficult to measure due to their transient nature and, as a consequence, their accuracy is usually quite low. In this study several inlet conditions were varied in order to investigate the sensitivity of results to their changes. Some of these conditions are the inlet solid volumetric fraction, the velocity profiles of the two phases, and the feeding mode of the solid. As already discussed earlier and illustrated in Figure 1, in the Miller and Gidaspow (1992) experiments, the feeding of solid and gas occurs through an inner tube at the riser bottom. A correct representation of this inlet geometry is crucial for a correct description of the lower part of the riser. For instance, a plug-flow feeding through the entire riser base, already implemented by some authors (Samuelsberg and Hjertager, 1996a,b), is unable to properly represent the lower section of the riser. As a consequence, several measurements have been carried out at the inlet section, such as solid velocity, volume fraction, and granular temperature. The data provided evidence of some accumulation of solid at the inlet tube wall. The associated velocity was also lower than the core velocity. As a consequence, in Simulation CFB-3, we imposed a trapezoidal profile for solid and gas velocity, and we assumed a concentration of 0.2 at the feeding-tube wall.

Figure 14 shows the solid volume fraction of Simulation CFB-3. The riser of Simulation CFB-3 is considerably denser than that of Simulation CFB-1 (see Figure 6b). Differences are quite evident both in the core and at the wall region. Radial profiles, similar to the ones reported in Figure 8, and not reported here for the sake of brevity, show significant differences between simulation and data values. The same effect can be detected from the granular temperature distribution for the two simulations. Its values are considerably lower for Simulation CFB-3 due to both the greater particle concentration in the riser and the smaller shear associated with lower velocities.

As a summary, the assumption of a trapezoidal velocity and solid concentration profiles seems to reduce the inlet momentum of the mixture, which is no longer able to describe the observed velocity field and turbulence production.

Effect of cohesive forces (Simulation CFB-4)

Cohesive forces due to the surface charge of particles are very important in the study of the behavior of small particles. Particles of few tens of microns in diameter are therefore subjected to this type of force. Gidaspow and Huilin (1998) have recently derived, from the radial distribution function of statistical mechanics, an expression for cohesive forces of 75-μm FCC particles. Since such a contribution increases with an increase of the solid volume fraction, it is of some interest to study its effect on the dynamics of the riser of a CFB.

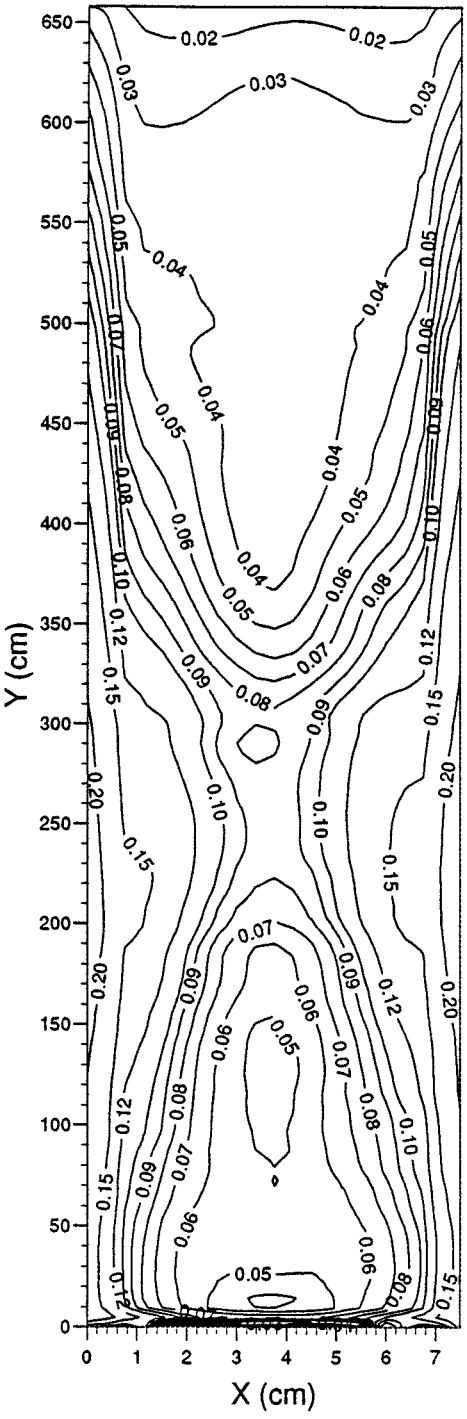

Figure 14. Time-averaged distribution of solid volumetric fraction for Simulation CFB-3.

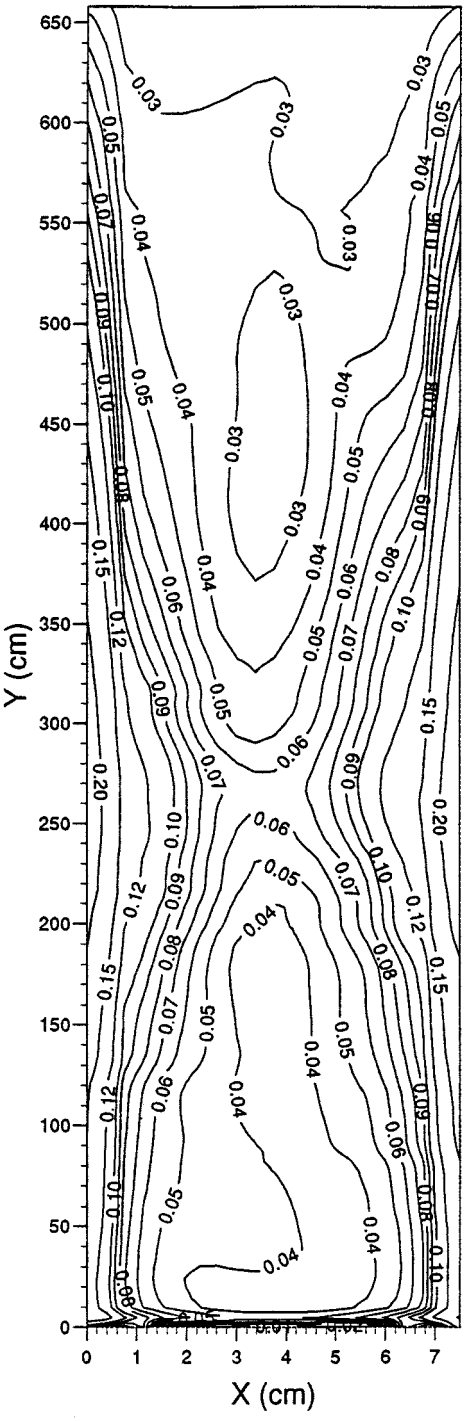

Figure 15. Time-averaged distribution of solid volumetric fraction for Simulation CFB-4.

In Simulation CFB-4, the cohesive pressure term has been added to the kinetic and collisional contributions. The final expression of the solid pressure is therefore

$$P_s = P_{\text{kin}} + P_{\text{coll}} + P_{\text{coh}} = \left[1 + 2(1+e)\epsilon_s g_0 - \left(0.73\epsilon_s + 8.957\epsilon_s^2\right)\right] \rho_s \epsilon_s \Theta. \quad (28)$$

Figure 15 shows the distribution of the solid volume fraction of Simulation CFB-4. Simulation results are consistent with the experimental data. Major differences with the distribution of Simulation CFB-1 are observed at the wall where the solid volume fraction is increased by about 5%. Minor changes are reported in the solid concentration in the core region where the volume particle fraction is below 5%.

Velocity distributions, not reported here, show minor differences with a slightly lower velocity for Simulation CFB-4. Same considerations apply to the granular temperature.

Influence of wall restitution coefficient (Simulation CFB-5)

With this simulation it is possible to investigate the influence of the restitution coefficient of the wall on the simulation results. The wall boundary conditions employed (Johnson and Jackson, 1987) allow the determination of the granular temperature at the wall based on the solution of a kinetic-energy balance at the wall. The knowledge of the restitution coefficient of the wall is therefore necessary for a correct application of the model. Gidaspow and Huilin (1998) estimated the restitution coefficient of the wall from measurement of granular temperature and solid volume fraction in the dilute regime of a CFB. By using the formula of Johnson and Jackson (1987), they derived a restitution coefficient of 0.96 for the acrylic tube of the IIT riser.

Figure 16 illustrates the distribution of the particle volume fraction of Simulation CFB-5. It is interesting to compare Simulation CFB-2 to Simulation CFB-5. They have been performed by using restitution coefficients of 0.96 and 0.8, respectively. From the figure it emerges that the wall restitution coefficient has some effect on the wall concentration, but its value is not critical for the definition of the flow pattern. In the case shown, a quite large variation of this parameter increases the wall concentration by only a small percentage and is unable to modify the dynamic behavior of the flow.

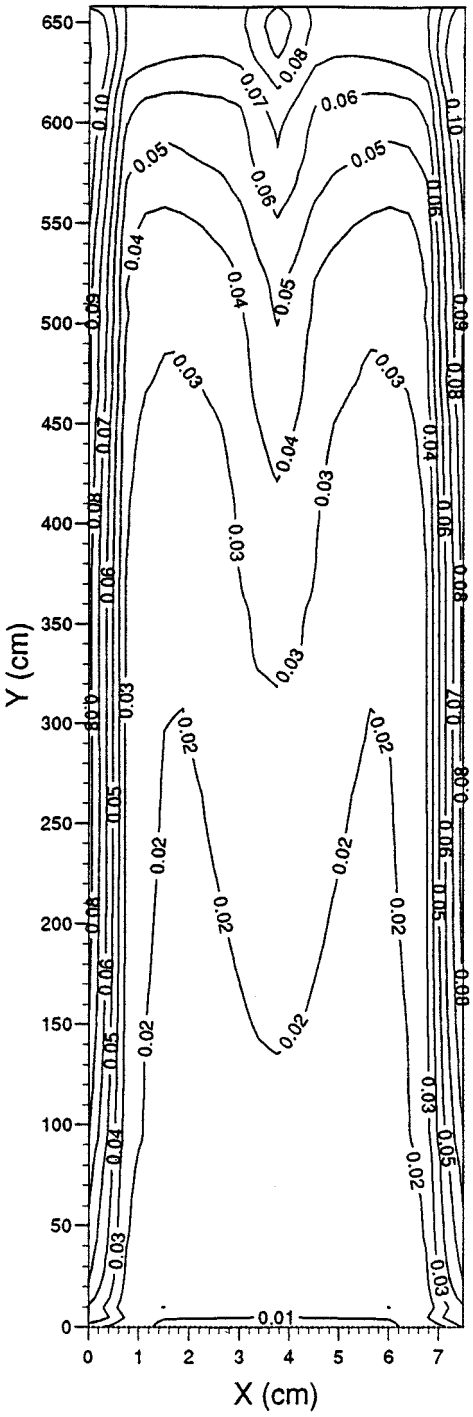

Figure 16. Time-averaged distribution of solid volumetric fraction for Simulation CFB-5.

Discussion and Conclusions

Three types of hydrodynamic models were used in the literature to predict riser flow: the viscosity model, the kinetic theory model with and without gas turbulence, and the k-epsilon model. The latter model is being developed at Los Alamos as part of the multiphase flow consortium. The model with solids viscosity as an input was used by Tsuo and Gidaspow (1989), Benyahia et al. (1998a), and by Sun and Gidaspow (1999) to model riser flow. The latter article describes the prediction of a new phenomenon not known to the fluidization community at the time of simulation: off-center maximum flux. The viscosity input model was used reasonably successfully to model flow patterns and bubbles in bubbling fluidized beds (Lyczkowski et al., 1993; Anderson et al., 1995). It appears that with a reasonable input of viscosity this model predicts the large-scale flow patterns and mixing on the order of equipment scale. It also appears to predict the slow oscillations, the gravity waves. It does not compute the small-scale oscillations with the scale length of the order of particle size. To do this, the present kinetic theory model was developed.

The kinetic theory model was first applied to developed riser flow in a pioneering article by Sinclair and Jackson (1989). Due to the assumption of steady developed flow, only ordinary differential equations were solved. The entrance region, the exit region, and the transient behavior characteristic of most fluidization were not computed. This study eliminates the assumptions made by Sinclair and Jackson and permits the solution of the more general problem. The commercial computer code FLUENT has a feature to use the kinetic theory, and has been shown to correctly predict some features of the core-annular flow regime for the PSRI challenge problem (Benyahia et al., 1998b).

In this article we show that the model computes the flow regime in a reasonable agreement with our experiment. The model is able to describe the most significant features of the two-phase flow riser hydrodynamics, the oscillatory-type motion of dense clusters, the time-averaged core-annular flow

regime, and the radial and axial nonhomogeneities of the flow. Radial solids concentrations, velocities and fluxes are consistent with measurements at three different sections. For the first time, the transient behavior of the riser has been compared here to experimentally measured large-scale frequencies of density oscillations. The computed and the measured frequency of the gravity wave is about 0.2 Hz. The computations show that the solids move in the form of clusters, which is consistent with observations.

The best comparisons between model predictions and data are obtained by using a two-dimensional Cartesian coordinate system with nonsymmetry imposed at the riser axis. The imposition of symmetry resulted in a wrong particle distribution due to a mirror effect. At volume fractions of about 3–4%, where most of the data are clustered, the computed granular temperature and the solids viscosity are in a good agreement with the experiment. In the dense region they disagree, probably due to the use of a constant restitution coefficient. The implementation of correct inlet conditions also appears to be critical for a successful simulation of flow hydrodynamics. Both feed geometry and flow conditions through the inlet cross section strongly affect the flow pattern in the riser. They need to be measured accurately. Output geometry and boundary conditions are equally important for a correct simulation of the flow behavior and need to be improved to achieve a better agreement between predictions and data.

The main advantage of the kinetic-theory model is that it gives the granular temperature—particle turbulence—and the viscosity in terms of first principles and physical parameters, such as particle size, allowing predictions to be made without extensive use of empirical correlations. Recently Buyevich and Cody (1998) have a made a very significant prediction using a slightly modified kinetic theory (Buyevich, 1999). In agreement with Cody's acoustic-probe granular-temperature measurements, they find that the granular temperature has a maximum value for a particle diameter of about 90 μm and a minimum of 150 μm. They use the high value of the granular temperature for Geldard A particles to explain the suppression of bubbles below minimum bubbling velocity. For both small and large particles the granular temperature increases with particle size. This behavior can be explained from the fluctuating energy balance for particles given in this article and in Gidaspow (1994, eq. 10.12). The equation shows the granular temperature to be proportional to particle diameter times velocity gradient squared. If we approximate the gradient by gas velocity minus the terminal velocity divided by pipe radius, we see that the granular temperature is the product of an increasing function of diameter times a decreasing function, since the terminal velocity increases with particle size. Hence we can explain the essence of Cody's discovery using kinetic theory only. To reach definitive conclusions, the code must be applied to other particle sizes.

Acknowledgments

This work was partially supported by the National Science Foundation (USA), Fluid, Particulate and Hydraulic Systems, and Consiglio Nazionale delle Ricerche, Gruppo Nazionale per la Vulcanologia (Italy), and European Community, Projects No. ENV4-CT98-0699 and ENV4-CT98-0703.

Notation

A, B = auxiliary constants
d = particle diameter
D = riser diameter
D_f = riser inlet diameter
e = restitution coefficient
g = gravitational acceleration
H = physical-domain height
L = physical-domain length
n = normal direction
q = granular temperature flux
r = radial coordinate
$\tilde{R}$ = gas constant
Re = Reynolds number
t = time
u = vertical component of velocity
$\boldsymbol{v}$ = velocity vector
x = horizontal coordinate
y = vertical coordinate
z = axial coordinate
ϵ = volumetric fraction
$\epsilon_{s,max}$ = maximum solid packing
λ = slip parameter
ρ = density
σ = shear stress
τ = stress tensor
Θ = granular temperature

Subscripts

coh = cohesive
coll = collisional
g = gas phase
in = inlet
kin = kinetic
out = outlet
slip = slip between the particle and the wall

Literature Cited

Ahmadi, G., and D. Ma, "A Thermodynamical Formulation for Dispersed Multiphase Turbulent Flows: I," *Int. J. Multiphase Flow*, **16**, 323 (1990).

Anderson, K., S. Sundaresan, and R. Jackson, "Instabilities and the Formation of Bubbles in Fluidized Beds," *J. Fluid Mech.*, **303**, 327 (1995).

Arastoopour, H., and D. Gidaspow, "Analysis of IGT Pneumatic Conveying Data and Fast Fluidization Using a Thermodynamic Model," *Powder Technol.*, **22**, 77 (1979a).

Arastoopour, H., and D. Gidaspow, "Vertical Pneumatic Conveying Using Four Hydrodynamic Models," *Ind. Eng. Chem. Fundam.*, **18**, 123 (1979b).

Arastoopour, H., P. Pakdel, and M. Adewumi, "Hydrodynamic Analysis of Dilute Gas-Solid Flow in a Vertical Pipe," *Powder Technol.*, **62**, 163 (1990).

Arastoopour, H., and H. Sue-Kim, "Numerical Analysis of Dilute Gas Particles Flow Using the Kinetic Theory," *Multiphase Flow Systems Simulations*, FED Vol. 199, ASME, New York (1994).

Avidan, A. A., "Fluid Catalytic Cracking," *Circulating Fluidized Beds*, J. R. Grace, A. A. Avidan, and T. M. Knowlton, eds., Blackie, London, p. 466 (1997).

Bader, R., J. Findlay, and T. M. Knowlton, "Gas-Solid Flow Patterns in a 30.5 cm Diameter Circulating Fluidized Bed," *Circulating Fluidized Bed Technology*, Vol. II, P. Basu and J. F. Large, eds., Pergamon Press, New York (1988).

Benyahia, S., H. Arastoopour, and T. M. Knowlton, "Prediction of Solids and Gas Flow Behavior in a Riser Using a Computational Multiphase Flow Approach," *Proc. Eng. Found. Conf. Fluidization*, Durango, CO (1998a).

Benyahia, S., H. Arastoopour, T. M. Knowlton, and H. Massah, "Simulation of Particle and Gas Flow Behavior in the Riser Section of a Circulating Fluidized Bed Using the Kinetic Theory Ap-

proach for the Particulate Phase,'' *Advanced Technologies for Particle Processing*, Vol. 2, Particle Technology Forum, AIChE, New York, p. 477 (1998b).
Buyevich, Y. A., and G. D. Cody, ''Particle Fluctuations in Homogeneous Fluidized Beds,'' Brighton World Congress on Particle Technology, Brighton, UK, Preprint, p. 3 (1998).
Buyevich, Y. A., ''Particle Stresses in Dense Disperse Flow,'' *Ind. Eng. Chem. Res.*, **38**, 731 (1999).
Cao, J., and G. Ahmadi, ''Gas-Particle Two-Phase Turbulent Flow in a Vertical Duct,'' *Int. J. Multiphase Flow*, **21**, 1203 (1995).
Capes, C., and K. Nakamura, ''Vertical Pneumatic Conveying: An Experimental Study with Particles in the Intermediate and Turbulent Flow Regimes,'' *Can. J. Chem. Eng.*, **51**, 31 (1973).
Chapman, S., and T. G. Cowling, *The Mathematical Theory of Nonuniform Gases*, Cambridge Univ. Press, London (1970).
Crowe, C., M. Sommerfeld, and Y. Tsuji, *Multiphase Flows with Droplets and Particles*, CRC Press, Boston (1998).
Davidson, J. F., ''Symposium on Fluidization: Discussion,'' *Trans. Inst. Chem. Eng.*, **39**, 230 (1961).
Ding, J., and D. Gidaspow, ''A Bubbling Fluidization Model Using Kinetic Theory of Granular Flow,''*AIChE J.*, **36**, 523 (1990).
Geldart, D., and M. J. Rhodes, ''From Minimum Fluidization to Pneumatic Transport: A Critical Review of the Hydrodynamics,'' *Circulating Fluidized Bed Technology*, P. Basu, ed., Pergamon Press, Oxford (1986).
Gidaspow, D., *Multiphase Flow and Fluidization: Continuum and Kinetic Theory Descriptions*, Academic Press, New York (1994).
Gidaspow, D., and L. Huilin, ''Collisional Viscosity of FCC Particles in a CFB,'' *AIChE J.*, **42**, 2503 (1996).
Gidaspow, D., and L. Huilin, ''Equation of State and Radial Distribution Function of FCC Particles in a CFB,'' *AIChE J.*, **44**, 279 (1998).
Gidaspow, D., U. K. Jayaswal, and J. Ding, ''Navier-Stokes Equations Model for Liquid-Solid Flows Using Kinetic Theory,'' *Liquid-Solid Flows*, FED Vol. 118, ASME, New York (1991).
Gidaspow, D., R. Bezbaruah, and J. Ding, ''Hydrodynamics of Circulating Fluidized Beds: Kinetic Theory Approach,'' *Fluidization*, Vol. VII, O. E. Potter and D. J. Nicklin, eds., Engineering Foundation, New York (1992).
Gidaspow, D., L. Huilin, and A. Therdthiangwong, ''Measurements and Computation of Turbulence in a Circulating Fluidized Bed,'' *Proc. Eng. Found. Conf. Fluidization*, Tours, France, published by Engineering Foundation, p. 81 (1995).
Gidaspow, D., L. Huilin, A. Neri, Y. Wu, and M. R. Mostofi, ''Turbulence Viscosity and Numerical Simulation of FCC Particles in CFB,'' *Proc. Fluidization and Fluid-Particle Systems*, Los Angeles, AIChE, New York, p. 58 (1997).
Harlow, F. H., and A. A. Amsden, ''Numerical Calculation of Multiphase Fluid Flow,'' *J. Comput. Phys.*, **17**, 19 (1975).
Hjertager, B. H., V. Mathiesen, and T. Solberg, ''Computational Analysis of Some Fluidized Systems,'' *Advanced Technologies for Particle Processing*, Vol. 2, Particle Technology Forum, AIChE, New York, p. 462 (1998).
Hui, K., P. K. Haff, J. E. Ungar, and R. Jackson, ''Boundary Conditions for High Shear Grain Flows,'' *J. Fluid Mech.*, **145**, 223 (1984).
Huilin, L., D. Gidaspow, and J. X. Bouillard, ''Dimension Measurements of Hydrodynamic Attractor in Circulating Fluidized Beds,'' *Powder Technol.*, **90**, 179 (1997).
Jackson, R., ''The Mechanics of Fluidized Bed: I. The Stability of the State of Uniform Fluidization,'' *Tran. Inst. Chem. Eng.*, **41**, 13 (1963).
Jackson, R., ''Progress Toward a Mechanics of Dense Suspensions of Solid Particles,'' AIChE Symp. Ser., Vol. 90, AIChE, New York, p. 1 (1993).
Jin, Y., J. X. Zhu, and Z. Q. Yu, ''Novel Configurations and Variants,'' *Circulating Fluidized Beds*, J. R. Grace, A. A. Avidan, and T. M. Knowlton, eds., Blackie, London, p. 525 (1997).
Johnson, P. C., and R. Jackson, ''Frictional-Collisional Constitutive Relations for Granular Materials, with Application to Plane Shearing,'' *J. Fluid Mech.*, **176**, 67 (1987).
Knowlton, T. M., ''Comparison of CFB Hydrodynamics Models. PSRI Challenge Problem,'' Int. Fluidization Conf., Tour, France (1995).
Kuipers, J. A. M., K. J. van Duin, F. P. H. van Beckum, and W. M. P. van Swaaij, ''A Numerical Model of Gas-Fluidized Beds,'' *Chem. Eng. Sci.*, **47**, 1913 (1992).
Lun, C. K. K., S. B. Savage, D. J. Jeffrey, and N. Chepurnity, ''Kinetic Theories for Granular Flow: Inelastic Particles in Couette Flow and Slightly Inelastic Particles in a General Flow Field,'' *J. Fluid Mech.*, **140**, 223 (1994).
Lyczkowsky, R. W., I. K. Gamwo, F. Dobran, H. Ali, B. T. Chao, M. M. Chen, and D. Gidaspow, ''Validation of Computed Solids Hydrodynamics and Pressure Oscillation in a Bubbling Atmospheric Fluidized Bed,'' *Powder Technol.*, **76**, 65 (1993).
Martin, M. P., P. Turlier, J. R. Bernard, and G. Wild, ''Gas and Solid Behavior in Cracking Fluidized Beds,'' *Powder Technol.*, **70**, 249 (1992).
Miller, A., ''Dense, Vertical Gas-Solid Flow in a Pipe,'' PhD Thesis, Illinois Institute of Technology, Chicago (1991).
Miller, A., and D. Gidaspow, ''Dense, Vertical Gas-Solid Flow in a Pipe,'' *AIChE J.*, **38**, 1801 (1992).
Neri, A., ''Multiphase Flow Modeling and Simulation of Explosive Volcanic Eruptions,'' PhD Thesis, Illinois Institute of Technology, Chicago (1998).
Rhodes, M. J., and D. Geldart, ''A Model for the Circulating Fluidized Bed,'' *Proc. AIChE Meeting*, Miami Beach, FL (1986).
Rivard, W. C., and M. D. Torrey, ''K-FIX: A Computer Program for Transient, Two-Dimensional, Two-Fluid Flow,'' Los Alamos National Laboratory, LA-NUREG-6623, Los Alamos, NM (1977).
Roco, M. C., ed., ''Advanced Technologies for Particle Processing,'' Particle Technology Forum, AIChE, Miami Beach, FL (1998).
Samuelsberg, A., and B. H. Hjertager, ''An Experimental and Numerical Study of Flow Patterns in a Circulating Fluidized Bed Reactor,'' *Int. J. Multiphase Flow*, **22**, 575 (1996a).
Samuelsberg, A., and B. H. Hjertager, ''Computational Modeling of Gas/Particle Flow in a Riser,'' *AIChE J.*, **42**, 1536 (1996b).
Sinclair, J. L., and R. Jackson, ''Gas-Particle Flow in a Vertical Pipe with Particle-Particle Interactions,'' *AIChE J.*, **35**, 1473 (1989).
Soo, S. L., *Fluid Dynamics of Multiphase Systems*, Blaisdell-Ginn, Waltham, MA (1967).
Squires, A. M., M. Kwauk, and A. A. Avidan, ''Fluid Beds: At Last, Challenging Two Entrenched Practices,'' *Science*, **230**, 1329 (1985).
Sun, B., and W. J. Koves, ''Application of a Numerical Hydrodynamic Model in FCC Design,'' *Particle Technology Forum*, Vol. 2, AIChE, Miami Beach, FL, p. 469 (1998).
Sun, B., and D. Gidaspow, ''Computation of Circulating Fluidized-Bed Riser Flow for the Fluidization VIII Benchmark Test,'' *Ind. Eng. Chem. Res.*, **38**, 787 (1999).
Syamlal, M., W. Rogers, and T. J. O'Brien, ''MFIX Documentation,'' U.S. Dept. of Energy, Federal Energy Technology Center, Morgantown, WV (1993).
Therdthianwong, A., and D. Gidaspow, ''Hydrodynamics and SO2 Sorption in a CFB Loop,'' *Circulating Fluidized Bed Technology*, Vol. IV, A. A. Avidan, ed., *Proc. AIChE Int. Conf. on Circulating Fluidized Beds*, New York, p. 551 (1994).
Thompson, T. B., ''Multiphase Fluid Dynamics Research Consortium,'' Fluid-Particle Interactions V, Santa Fe, NM (1999).
Tsuo, Y. P., and D. Gidaspow, ''Computation of Flow Patterns in Circulating Fluidized Beds,'' *AIChE J.*, **36**, 885 (1990).
Weinstein, H., M. Shao, M. Schnitzlein, and R. A. Graff, ''Radial Variation in Void Fraction in a Fast Fluidized Bed,'' *Fluidization*, Vol. V, K. Ostergaard and A. Sorensen, eds., Engineering Foundation, New York (1986).

Manuscript received Jan. 18, 1999, and revision received July 14, 1999.